ACS APPLIED ELECTRONIC MATERIALS

pubs.acs.org/acsaelm

Article

Submicrometer Spatially Controlled Doping of Polymer Thin Films by a Single-Step Soft-Contact Approach

Denis Gentili,* Margherita Bolognesi,* Matteo Baldoni, Francesco Mercuri, Michele Muccini, and Massimiliano Cavallini

Cite This: *ACS Appl. Electron. Mater.* 2023, 5, 6996−7003

Read Online

ACCESS | Metrics & More | Article Recommendations | Supporting Information

ABSTRACT: Polymer thin films have become increasingly popular for the fabrication of large-area and flexible devices. Doping of organic thin films is a powerful strategy to achieve highly efficient devices with precise and reliable control of their key parameters and to expand their range of applications. However, the spatially controlled doping of polymer thin films is a challenging task that has yet to be adequately addressed. Herein, we report an effective strategy for local doping of polymer thin films with submicrometer lateral resolution in a single step. We use optically inert poly(methyl methacrylate) (PMMA) and blue-fluorescent poly(9,9-di-n-octylfluorenyl-2,7-diyl) (F8 or PFO) thin films as models to investigate the doping process with different photoluminescent dyes (Rhodamine 101, Fluorescein 27, Coumarin 2 and DCM) by fluorescence microscopy, laser scanning confocal microscopy and localized and photoluminescence spectroscopy. Further insights into the doping mechanism are provided by computational studies. We show that the use of soft stamps as spatially confined doping tools allows for localized doping of the polymer thin film through dye diffusion without compromising the film morphology. This strategy overcomes solvent compatibility constraints typical of organic material processing and can be additive, allowing thin films to be doped with multiple dyes with independent control over their spatial distribution. These results strongly support the effectiveness of stamp-assisted doping as a highly versatile and reliable approach for achieving the spatially controlled doping of polymer thin films, thereby opening opportunities for organic optical and optoelectronic applications.

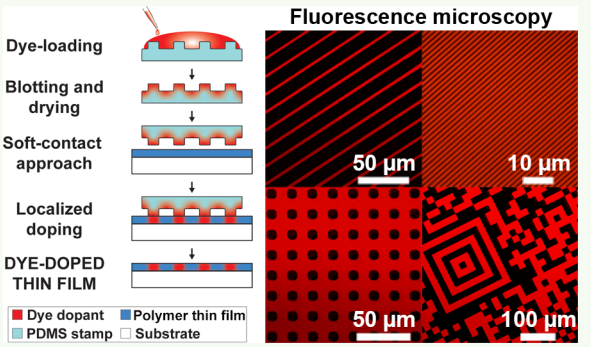

KEYWORDS: *spatially controlled doping, thin film polymer, soft stamp, dye diffusion, confocal fluorescence micro-spectroscopy*

INTRODUCTION

The growing interest in the application of organic materials in electronic, photonic, and optoelectronic devices is due to the possibility to tailor their properties in combination with low manufacturing cost, flexibility, lightweight, solution and large-area processability, and low-temperature manufacturing.[1−5] Other than single devices, the miniaturization and integration of efficient organic electronics and optoelectronics have also enabled the development and demonstration of sensing systems for the point-of-need.[6,7] Tailoring the optical, electrical, and optoelectronic properties of organic materials can be pursued through chemical design,[8−10] control of their polymorphic phases,[11,12] and the addition of molecular dopants.[13,14] Similar to their inorganic counterpart, doping of organic semiconductors is emerging as an indispensable strategy to achieve highly efficient devices with precise and reliable control of their key parameters.[15−18] The soft nature of organics compared to that of inorganic materials makes them suitable for otherwise inaccessible applications, but it also makes them incompatible with typical doping processes. Alternative doping strategies for organic materials have been proposed to increase the performance of organic transistors and to control the emission color of polymer light-emitting devices.[19−23] The easiest and cheapest manufacturing processes for doping organic thin films include solution-based techniques such as coprocessing or immersion, thermal or chemical vapor doping, electrochemical doping, or physisorption.[24−26] Controlling the doping process of organics in organics is a complex task, and different alternatives have been explored. Doping by codeposition is the simplest method and allows a fine control of the dopant concentration, but it does not allow spatial confinement of the dopant in the host film. In addition, codeposition from solution-based techniques may pose solubility constraints and typically lacks a fine control on the resulting film microstructure (contrarily to codeposition from vapor-based techniques). Alternative sequential processing methods, based on the addition of the dopant into a

Received: October 2, 2023
Revised: November 14, 2023
Accepted: November 20, 2023
Published: December 7, 2023

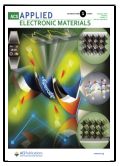

preexisting host film, include vapor, electrochemical, or immersion doping. A limitation of sequential processing methods is that the dopant diffusion in the host matrix depends on the thickness and porosity of the host film and on the diffusion coefficient of the dopant. However, the structural order of the host film is more easily retained during the doping process, and patterned doping is also possible. In the case of vapor doping, spatial control of the doping can be achieved by the use of shadow masks. However, the resolution and definition of the doping spatial features are determined by the (expensive and complicated) technologies used for the fabrication, positioning, application, and removal of shadow masks. On the other hand, patterned doping from alternative dry or solution-based techniques has been less explored. Therefore, cheap and versatile alternatives for the spatially controlled doping of functional organic layers must be addressed, to fully meet the technological aspirations placed on the use of these materials.[13] While several examples of homogeneous doped thin films obtained by blending and coating/dipping have been reported,[25,27−30] there is no established methodology to achieve the spatially controlled doping of submicrometric areas of organic thin films. The solution processability of organic materials allows the use of low-cost manufacturing processes but also poses solvent compatibility issues when multistep processing strategies are required. Controlled spatial wet deposition of the dopant requires the selection of orthogonal solvents for the dopant and the material to be doped so as not to compromise the predeposited organic film. Solvent compatibility/orthogonality constraints severely limit the successful doping of organic thin films with controlled spatial resolution. Despite the plurality of versatile and low-cost nonphotolithographic techniques capable to pattern at micro and nanoscale a wide range of functional materials, such as soft lithographic techniques,[31,32] few studies have reported localized molecular doping of organic layers. These strategies exploit the diffusion of dopant molecules from a "donor substrate" to the target polymer film using masks, localized Joule heating or silicon stamps, and, more recently, by inkjet printing, local dedoping, or the combination of an interlayer and laser light stimuli to spatially control the doping process.[33−41]

In the present work, we report on the submicrometer spatially controlled doping of polymer thin films with a dye by means of a stamp-assisted, additive, and soft-contact technique. We demonstrate that the use of soft stamps as a dopant-donor substrate is an effective strategy for locally doping polymer thin films with submicrometer lateral resolution in a single step. As schematically shown in Figure 1a, spatially controlled doping is performed using elastomeric stamps that have the dual function of acting as a molecular dopant reservoir and imposing lateral confinement of the doping process. The soft contact with the relief structures of the stamp allows localized doping of the polymer thin film through dye diffusion without compromising the film morphology. We investigate the doping process in optically inert poly(methyl methacrylate) (PMMA) and blue-fluorescent poly(9,9-di-n-octylfluorenyl-2,7-diyl) (F8 or PFO) with different photoluminescent dye dopants by fluorescence microscopy, laser scanning confocal microscopy (LSCM), and localized and photoluminescence (PL) spectroscopy. The use of an inert and transparent polymer, such as PMMA, allows us to demonstrate the spatially controlled doping by exploiting the optical properties of three different commercial dyes (Rhodamine 101, Fluorescein 27, and Coumarin 2) without any interference from the surrounding host material. Moreover, the investigation of composition-dependent photophysical properties of fluorescent F8 thin films doped with the charge transfer emitting dye 4-(dicyanomethylene)-2-methyl-6-(4-dimethylaminostyryl)-4H-pyran (DCM) provides deeper insights into the doping process. Finally, further insights into the doping mechanism and on the dynamics of the process are provided by computational studies.

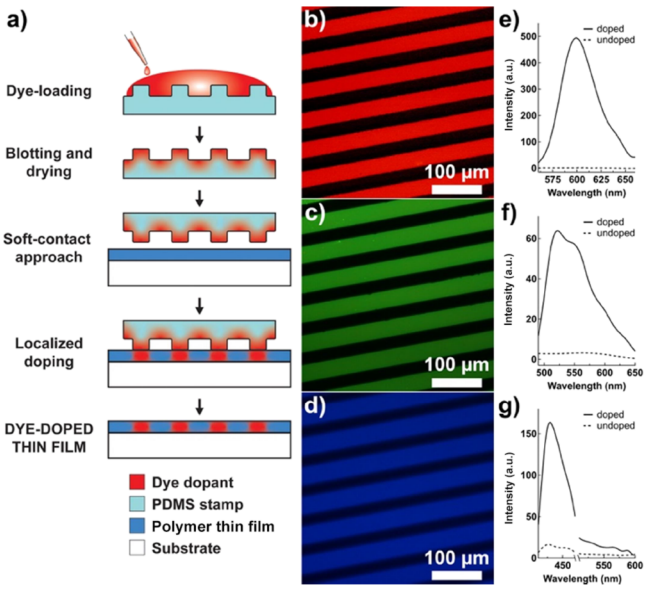

Figure 1. (a) Schematic representation of stamp-assisted and soft-contact doping process. Fluorescence microscope images and corresponding localized emission spectra (light excitation: 405 nm) of PMMA thin films doped with (b, e) Rhodamine 101 (Ex 510−560 nm, DM 575 nm, BA 590 nm), (c, f) Fluorescein 27 (Ex 400−440 nm, DM 455 nm, BA 470 nm), and (d, g) Coumarin 2 (Ex 330−380 nm, DM 400, BA 420).

EXPERIMENTAL SECTION

Materials. 4-(dicyanomethylene)-2-methyl-6-(4-dimethylaminostyryl)-4H-pyran (DCM, 98%), PMMA (M_w ~ 120,000), chloroform (anhydrous, 99.8%), toluene (anhydrous, 99.8%), butyl acetate (anhydrous, 99%), isopropyl alcohol (spectrophotometric grade, 99.5%), and ethylbenzene (anhydrous, 99.8%) were bought from Merck. Rhodamine 101, Fluorescein 27, and Coumarin 2 were bought from Exciton. Poly(9,9-di-n-octylfluorenyl-2,7-diyl) (F8 or PFO, M_w = 58,000, PDI = 2.7) was bought from Ossila Ltd. Sylgard 184 (polydimethylsiloxane, PDMS) silicone elastomer base and the curing agent were purchased from Dow Corning.

Thin Film Preparation. Thin films of PMMA or F8 were deposited onto quartz or Si/SiOx substrates by spin coating (1500−3000 rpm) of a PMMA butyl acetate solution (20 g/L) or F8 toluene solution (5 or 10 g/L) under inert atmosphere of nitrogen (O_2 < 0.1 ppm, H_2O < 0.1 ppm). Thin films with thicknesses of 20, 40, and 60 nm were prepared varying the F8 or PMMA concentration and controlling deposition conditions. The solvent is allowed to evaporate at room temperature for 24 h. Before the deposition, the substrates were cleaned by sonication in acetone, in 2-propanol, and then dried under a stream of nitrogen.

Doping. Doping of PMMA films with Rhodamine 101, Fluorescein 27, and Coumarin 2, and doping of F8 films with DCM were performed by the stamp-assisted soft-contact doping technique. Elastomeric PDMS molds were prepared by replica molding of silicon masters fabricated by photolithography.[42] The stamp motifs consist of parallel lines (600 nm wide and 1.5 μm

https://doi.org/10.1021/acsaelm.3c01379
ACS Appl. Electron. Mater. 2023, 5, 6996−7003

periodicity, or 30 μm wide and 60 μm periodicity, or 2.5 μm wide and 15 μm periodicity), square grid (hole size 10 μm), or a matrix code. After curing for 6 h at 70 °C, PDMS stamps were peeled off, cleaned by sonication in ethanol for 10 min, and dried in a stream of nitrogen prior to use. The structured side of the PDMS stamp was brought into contact with a 1 g/L (or saturated) solution of dyes in chloroform at room temperature, and after 60 s, the excess of solution was removed by blotting with optical lens paper and then dried under a stream of nitrogen. The stamp was brought to and left in contact with the PMMA or F8 films under dry nitrogen. Afterward, the stamp was removed, and before characterization, the films were aged under a nitrogen atmosphere for 2 h.

Morphology Measurements. Atomic force microscopy (AFM) images were collected at room temperature in air on a Multimode 8 microscope operated in PeakForce mode and equipped with a type J scanner (Bruker Nano Inc. GmbH) and SNL-A probes (Bruker AFM Probes, Camarillo, CA). Background interpolation was performed with Gwyddion 2.61 (http://gwyddion.net/).[43] The morphology was quantitatively characterized via the root-mean-square surface roughness descriptor S_q. Reported S_q values are the averages of at least five different regions.

Optical Microscopy. Samples were examined using a Nikon Eclipse 80i microscope equipped for fluorescence analysis.

Profilometry. The thickness of the thin films was measured by a KLA Tencor $P\bar{6}$.

UV−vis Absorption. The absorption spectra of F8 and DCM in solution and of thin films on quartz were recorded with a Jasco V-550 spectrophotometer using bare quartz as the reference.

PL Spectroscopy. PL spectra of thin films were recorded by exciting the samples with laser sources at 375 or 442 nm and collecting emission with a PM-11 optical multichannel analyzer from Hamamatsu. All measurements were performed with the samples kept in a vacuum chamber ($\sim 10^{-5}$ mbar) at room temperature.

LSCM. The LCSM images were registered with a Nikon TE2000 inverted microscope, equipped with a laser diode source at 405 nm, a 60× objective with 0.70 numerical aperture, and a pinhole, connected with a Nikon EZ-C1 confocal scanning head. All measurements were performed with the samples kept in a vacuum chamber ($\sim 10^{-5}$ mbar) at room temperature.

Localized PL Spectroscopy. The localized PL spectra were acquired by optical coupling the LSCM output optical fiber with the PM-11 optical multichannel analyzer from Hamamatsu, selecting an acquisition area of 10 × 30 μm or 30 × 30 μm from the LCSM images by the EZ-C1 software.

Computational Studies. Finite-element simulations were performed by employing the COMSOL Multiphysics 6.0 simulation software (Burlington, MA, USA). After testing, the fine free triangular mesh was chosen for the modeling. The "Chemical Species Transport" module ("Transport of diluted species in porous media") has been used. Analyzing the results of computational and experimental studies about similar systems in the literature, the diffusion coefficients of both PDMS and PMMA were set to 10^{-13} m^2/s.[44,45] To account for the effect of porosity in the diffusivities, the Millington and Quirk models have been applied. The values of the porosity for the PDMS and PMMA were set at $\varepsilon_{PDMS} = 10^{-15}$, $\varepsilon_{PMMA} = 10^{-16}$, respectively. The study has been carried on in time-dependent mode, with timesteps of 1 min for a total simulation time of 1 h.

RESULTS AND DISCUSSION

Soft and elastomeric stamps made of PDMS were fabricated by replica molding of prepatterned masters.[42] We used stamps made of PDMS because it is an elastomer with low interfacial free energy and chemical inertness, which allows excellent conformal contact with surfaces and reversible adhesion.[46] The loading of the dopant into stamps was performed by bringing the patterned side in contact with chloroform solutions of the dye followed by a quick drying step to remove excess solution. Solution concentration, dipping, and drying time of the loading procedure have been optimized to minimize the formation of dye deposits that could compromise the homogeneity of the doping process by monitoring the surface morphology of the stamps by optical microscopy. The surface of the stamps appears, in fluorescence microscope images, almost free of deposits after the loading phase for all of the dyes used (Figure S1). Stamp-assisted doping was performed by bringing into contact for 1 h the patterned side of a dye-loaded stamp with 60 nm-thick PMMA films deposited on quartz or silicon substrates by spin coating (Figure 1a). The fluorescence microscope images shown in Figure 1b−d reveal the presence of Rhodamine 101 (red), Fluorescein 27 (green), and Coumarin 2 (blue) in the PMMA thin films only in the regions that were in contact with the stamp, as the doped areas exactly reproduce the stamp pattern. The localized PL spectra of the doped PMMA thin film (Figure 1e−g) confirm that dye diffusion occurs only in the contact regions between stamp protrusions and the polymer film, regardless of the dye. The dye-doped areas show emission spectra (Figure 1e−g solid lines) in agreement with the corresponding dye/PMMA blend films (Figure S2a−c), while no (or barely detectable) fluorescence is detected in the undoped areas (Figure 1e−g dashed lines). In particular, while no emission from the undoped areas is registered for the Rhodamine 101 based sample (Figure 1e, dashed line), a very low but detectable residual emission is registered from the undoped areas of the Fluorescein 27 based sample (Figure 1f, dashed line), and a slightly higher residue is registered in the undoped areas of the Coumarin 2 based sample (Figure 1g, dashed line). This trend could be explained by light scattering effects rather than by dye diffusion in the PMMA film outside the contact regions. Indeed, although scattering should be minimized using the pinhole in the confocal microscope setup, under the same experimental conditions used for the three systems, residual light scattering possibly still occurs and increases passing from the red spectral region to the green, to the blue one (Rayleigh scattering). In details, the ratio between the integrated spectra taken in the doped and in the undoped regions decreases passing from the red spectral region (ratio of 110 for Rhodamine 101) to the green spectral region (ratio of 15 for the Fluorescein 27) to the blue spectral region (ratio of 6 for Coumarin 2). In addition, it should be noted that we used the same stamp-film contact time (1 h) for all three dyes, but this may not be the optimal contact time to maximize the diffusion of the dye from the stamp to the polymer thin film, which varies depending on the specific combination of dye and polymer.

Overall, the edges of all the patterns are well-defined, and their structure and lateral resolution are dictated by the stamp motif. The doping process showed remarkable reproducibility, regardless of the dye used, and most noteworthy, the stamps were used at least 10 times with no observed deterioration in lateral resolution performance.

As an example, to assess the versatility of stamp-assisted doping, PMMA thin films were doped with Rhodamine 101 using stamps with three different patterns and lateral resolution. Figure 2a,b shows PMMA films doped with parallel Rhodamine lines of different widths and spacings from those shown in Figure 1b−d. We were able to achieve the localized doping of PMMA films in a single step with lateral resolution in the submicron scale, i.e., rhodamine-doped parallel lines 600 nm wide and 900 nm apart (Figure 2b), as well as to produce

https://doi.org/10.1021/acsaelm.3c01379
ACS Appl. Electron. Mater. 2023, 5, 6996−7003

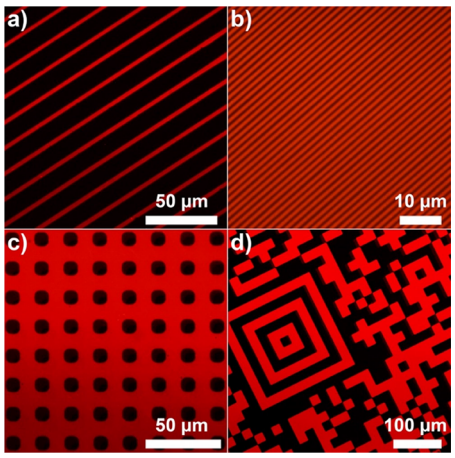

Figure 2. Fluorescence microscope images (Ex 510−560 nm, DM 575 nm, BA 590 nm) of PMMA thin films doped with Rhodamine 101 using stamps with different patterns: (a) parallel lines 2.5 μm wide and 15 μm periodicity, (b) parallel lines 600 nm wide and 1.5 μm periodicity, (c) square grid, and (d) matrix code.

dye-doped PMMA thin films with completely different patterns from the parallel lines, i.e., square grid (Figure 2c) and matrix code (Figure 2d). Noteworthy, AFM measurements revealed that the surface roughness (S_q) of PMMA thin films (S_q < 1 nm, scanning square areas of 5 μm × 5 μm) is unaffected by the doping process, and the film flatness is retained (Figure S3). The preservation of the host film microstructure is a peculiar feature of the proposed doping methodology, as compared to the other doping techniques from the literature where often either the dopant itself or the doping process has an observable impact on the film microstructure.[37,47−51]

These results indicate that, within the range studied, the main limitation affecting the pattern and lateral resolution of the stamp-assisted doping process is related to the challenges associated with producing stamps with specific patterns and lateral resolution and that the morphology of polymer thin films is not affected by the doping process.

We then investigated the additivity of the stamp-assisted dye-doping process by bringing twice the PMMA films into contact with dye-loaded stamps. As schematically shown in Figure 3a, we have used stamps consisting of linear protrusions, and following the first doping process, a second doping step was performed, either using the same dye or alternative ones, after a 90-degree rotation of the polymer thin film. As shown in Figure 3b−l, on PMMA films obtained by additive doping, areas doped with the first or second dye, doped with both dyes, and undoped coexist. In PMMA films doped both times with the same dye, the PL intensity of the intersection areas of the stripes, i.e., where the doping process took place twice, is higher than in the others, thus confirming the additivity of the stamp-assisted doping. Likewise, when PMMA films are doped with two different dyes in sequence, the intersection area exhibits a PL spectrum that is the sum of the spectra from the two dyes. Figure S4 displays the localized PL spectra of PMMA films doped with Rhodamine 101 and Fluorescein 27. The PL spectra from regions doped with a single dye are consistent with those of the respective single-dye-doped samples (refer to Figure 1), whereas the PL spectrum from regions where the PMMA is doped with both dyes is a combination of their spectra.

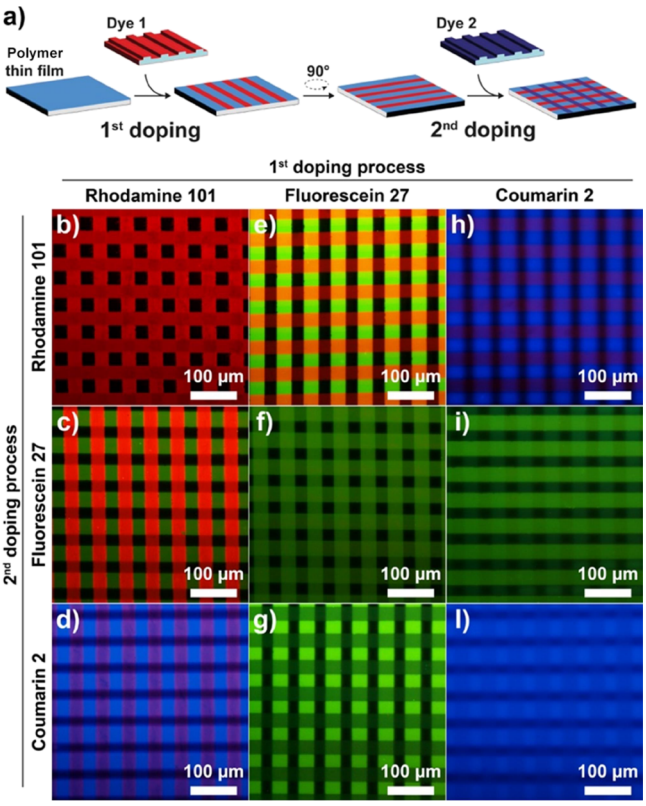

Figure 3. (a) Schematic representation of the additive doping process. (b) Fluorescence microscope images of PMMA thin films on which stamp-assisted doping was carried out twice using stamps consisting of parallel, linear protrusions 30 μm wide and 30 μm apart (first doping: vertical stripes; second doping horizontal stripes). The excitation/emission filter combination and acquisition time were adapted individually to better highlight the additive doping process. Fluorescence filters: Ex 330−380 nm, DM 400, BA 420 for images (d), (h), and (l); Ex 400−440 nm, DM 455 nm, BA 470 nm for images (c), (e), (f), (g), and (i); and, Ex 510−560 nm, DM 575 nm, BA 590 nm for image b.

To gain deeper insight into the mechanism of doping, we have investigated the stamp-assisted doping of thin films of a large-band gap fluorescent polymer (F8) with an environmentally sensitive emissive dye (DCM). DCM dyes have a typical donor−acceptor structure, resulting in a broad absorption from an ultrafast internal charge transfer,[52] and in a high-yield emissive charge transfer state (CT state). Indeed, DCM derivatives were introduced in the late 80s as highly fluorescent dopants in organic electroluminescent diodes.[53] The photophysical characteristics of the chosen system allow the study in more detail of the doping process by PL spectroscopy. Emission from the excited state of F8 competes with resonant energy transfer to the emissive CT state of DCM.[54] This is possible only if a large number of F8 and DCM molecules are close to each other at maximum intermolecular distance in the nanometer range, i.e., only if doping is effective. The CT nature of the DCM emissive state means that the photophysical characteristics of the system are also highly sensitive to the dopant concentration, which causes electronic perturbation of the CT state. A detailed photophysical study of F8:DCM blend films is reported in the Supporting Information (see Photophysical Study of F8:DCM Blend Films).

https://doi.org/10.1021/acsaelm.3c01379
ACS Appl. Electron. Mater. 2023, 5, 6996−7003

The role of polymer film thickness has been assessed by contacting flat, unpatterned DCM-loaded stamps with 20-, 40-, and 60 nm-thick F8 thin films deposited on quartz or silicon substrates. Figure 4a shows the PL spectra of F8 thin films after

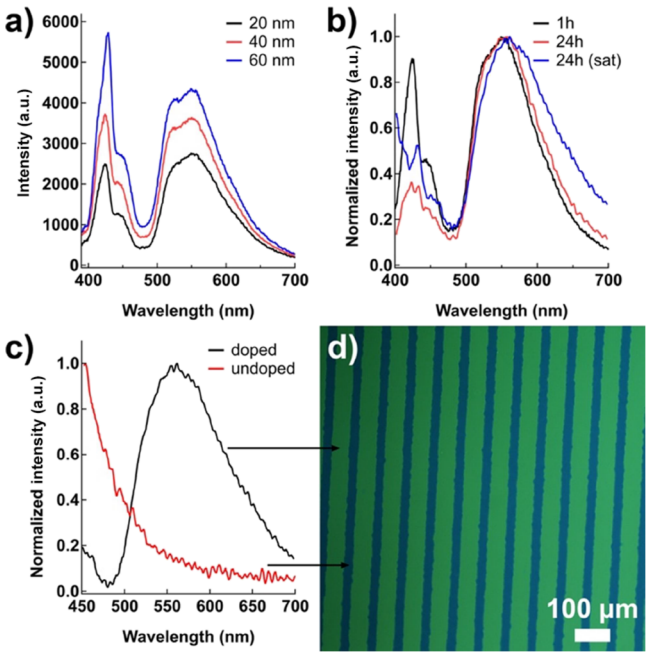

Figure 4. (a) PL spectra of F8 thin films with different thickness (20, 40, and 60 nm) doped with DCM by using flat, unpatterned stamps (contact time: 1h; light excitation: λ_{exc} = 375 nm); (b) normalized PL spectra (light excitation λ_{exc} = 375 nm) of F8 thin films (thickness: 20 nm) doped with DCM by using unpatterned stamps and different conditions: contact time 1 h (black line) or 24 h (red line) with stamps loaded with DCM by standard procedure; and, contact time 24 h with stamp loaded with DCM by immersion (blue line). (c) Localized PL spectra (light excitation: λ_{exc} = 405 nm). (d) Fluorescence microscope image (Ex 400−440 nm, DM 455 nm, BA 470 nm) of F8 thin film doped with DCM by using a stamp consisting of parallel lines 40 μm wide and 70 μm periodicity. Note that the emission spectra in (c) are cutoff at 450 nm due to the presence of a dichroic filter in the LSCM setup to eliminate the backscattered laser light excitation.

the same contact time (1 h) with the DCM-loaded stamp. The intensity of characteristic blue emission of F8, peaked at 438 nm, increases with the increase of the film thickness, as well as the band centered at around 550 nm, characteristic of emission from the CT state of DCM in an apolar environment. However, while intensity ratio between the emission peaks of DCM and F8 of 20- and 40 nm-thick thin films is almost the same (∼1), the thicker F8 film shows a lower ratio (∼0.75) as best evidenced by the normalized spectra (Figure S5). These results suggest that the doping concentration of the 60 nm-thick films is significantly lower than that achieved in the thinner films.

For further insights into the stamp-assisted doping process, we then investigated the effect of the stamp-film contact time and the amount of doping agent contained in the stamp at a fixed film thickness (20 nm). As shown in Figure 4b, the intensity ratio between the emission peaks of DCM and F8 doubled when the stamp-film contact time was increased from 1 h (black line) to 24 h (red line), revealing that the DCM concentration in the F8 thin film increases with increasing the contact time. It is noteworthy that the DCM molecules retained their isolated behavior (i.e., no bathochromic shift of the emission peak was observed) despite the increase in DCM concentration in the F8 film. A further increase of the stamp contact time to 72 h leads to a decrease of the absolute PL intensity, probably due to a degradation of the dye molecules during the prolonged contact time (data not shown).

We also investigated the effect of increasing the DCM concentration in stamps on the doping process by loading a 10 times more concentrated solution of DCM (i.e., 10 g/L). However, this led to the formation of micrometer aggregates on the stamp surface, thus compromising the possibility of achieving good contact between stamps and F8 films (data not shown). Therefore, the loading of DCM was increased by saturating the stamps through full immersion in a 1 g/L of DCM solution. The F8 films, which were doped using these stamps (i.e., saturated with DCM solution), show both a slight decrease in the ratio of the DCM peak to F8 and a bathochromic shift (from 554 to 561 nm) of the DCM peak (Figure 4b, blue line with respect to the red line). The findings imply that a higher load of DCM in the stamp promotes the diffusion of more DCM molecules into the F8 thin film and to a greater intermolecular proximity between DCM molecules in the film, leading to concentration effects (i.e., intermolecular electronic interactions) on the emission from their CT state. Finally, as for PMMA films, spatially controlled doping of F8 thin films with DCM has been performed using patterned stamps consisting of parallel, linear protrusions 40 μm wide and 70 μm periodicity. The optical properties of the resulting samples were then characterized by using LSCM and localized PL spectroscopy. Figure 4c shows the localized PL spectra of the DCM-doped F8 film shown in Figure 4d. The emission spectrum of the polymer film areas that were in contact with the stamp protrusions (black line, Figure 4c) matches perfectly with that of the DCM-doped F8 shown in Figure 4b, while only the emission of pristine F8 is detected in the other regions (red line, Figure 4c). These results further confirm that the diffusion of dye from the stamp to the host thin film is confined to the stamp-film contact regions.

Finally, finite-element simulations were performed to reproduce the diffusion process of the dye molecules at the stamp−film contact interface (Figure 5a). The model is composed of two domains where the upper trapezoid represents the dye-loaded PDMS stamp and the lower rectangular region represents the PMMA thin film (see Figure S6a for the domain dimensions). Due to their comparable molecular weights, nearly planar conformations, and similar polarities, we assumed identical diffusion coefficients for the investigated dyes. At t = 0, the initial dye concentration in the stamp is equal to the nominal concentration of the solution (1 g/L, approximately 2.2 × 10^{-3} M), while the polymer film contains no dye (c = 0 M). The analysis of the concentration profile at different contact times, specifically after 6, 30, and 45 min (Figure S6b−d), demonstrates an increasing diffusion of dye from the PDMS stamp to the polymer thin film. In excellent agreement with the experimental results, after 1 h (the contact time used for the experiments), the concentration profile showed in Figure 5b exhibits a significant transfer of the dye exclusively to the PMMA area in direct contact with the PDMS stamp, while the concentration diminishes to almost negligible levels at a distance of 70 nm away from the point of contact.

https://doi.org/10.1021/acsaelm.3c01379
ACS Appl. Electron. Mater. 2023, 5, 6996−7003

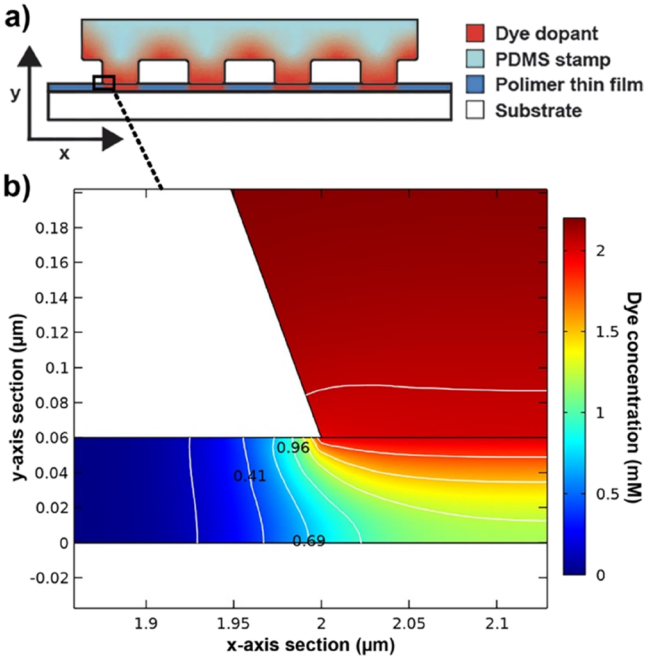

Figure 5. (a) Schematic representation of the stamp-film section. (b) Concentration profile plot on a section of the model perpendicular to the PMMA substrate after 1 h of contact with the dye-loaded PDMS stamp. The trapezoidal domain represents the PDMS mold, while the rectangular one is the PMMA substrate.

Overall, our study provides compelling evidence supporting the effectiveness and reliability of stamp-assisted doping as a viable strategy for achieving precise spatial control over molecular doping in polymer thin films.

CONCLUSIONS

In conclusion, this study presents a novel and effective method to achieve spatially controlled doping of polymer thin films with submicrometer lateral resolution in a single step. The use of soft stamps as doping tools, combined with the high-resolution lateral confinement, allows for localized doping of the polymer thin film through dye diffusion without compromising the film morphology. We successfully demonstrated this process on various model systems, including optically inert PMMA and fluorescent F8 polymer thin films with four different photoluminescent dyes as dopants. Moreover, we demonstrated the feasibility of additive and sequential film doping with different dyes, each with an independently controlled spatial distribution. Fluorescence microscopy and localized PL spectroscopy were employed to investigate the stamp-assisted doping process, while AFM studies revealed that it has no detrimental effect on the surface morphology of the polymer films. By employing LSCM and localized PL spectroscopy on the F8 polymer doped with the DCM dye, which has environment- and concentration-dependent photophysical properties, we gained further insights into the effects of polymer film thickness, stamp-film contact time, and dopant concentration in the stamp on the doping process. Our experimental results, along with computational studies, indicated that the doping process occurs through dye diffusion from the stamp to the polymer thin film. Overall, the results of this study strongly support the effectiveness of stamp-assisted doping as a highly versatile and reliable approach for the spatially controlled doping of polymer thin films. This strategy overcomes the solvent compatibility constraints typically associated with organic material processing and can be repeated multiple times, allowing for the doping of thin films with multiple dyes while maintaining an independent control over their spatial distribution. Additionally, the flexibility of this method, which does not rely on specific chemical or physicochemical properties of the polymer thin film, makes it a versatile and promising approach for a wide range of materials, including high-performance conjugated polymers. In summary, by addressing the challenge of spatially controlled doping of organic thin films, the soft stamp doping technique demonstrated here holds great promise for future applications in various technological fields that rely on the tailored properties of polymer thin films, such as electronic, photonic, and optoelectronic devices. Furthermore, the low-cost and solution-based nature of the doping process makes it an attractive manufacturing strategy for large-area and flexible devices.

ASSOCIATED CONTENT

Supporting Information

The Supporting Information is available free of charge at https://pubs.acs.org/doi/10.1021/acsaelm.3c01379.

Additional photoluminescence spectra, localized emission spectra and image, and concentration profile plots; fluorescence microscope images of PDMS stamp, AFM images, photoluminescence spectra of blend films and photophysical study of F8:DCM blend films (PDF)

AUTHOR INFORMATION

Corresponding Authors

Denis Gentili − *Consiglio Nazionale delle Ricerche, Istituto per lo Studio dei Materiali Nanostrutturati (CNR-ISMN), 40129 Bologna, Italy;* orcid.org/0000-0002-7599-2804; Email: denis.gentili@cnr.it

Margherita Bolognesi − *Consiglio Nazionale delle Ricerche, Istituto per lo Studio dei Materiali Nanostrutturati (CNR-ISMN), 40129 Bologna, Italy;* orcid.org/0000-0003-0080-3279; Email: margherita.bolognesi@cnr.it

Authors

Matteo Baldoni − *Consiglio Nazionale delle Ricerche, Istituto per lo Studio dei Materiali Nanostrutturati (CNR-ISMN), 40129 Bologna, Italy*

Francesco Mercuri − *Consiglio Nazionale delle Ricerche, Istituto per lo Studio dei Materiali Nanostrutturati (CNR-ISMN), 40129 Bologna, Italy;* orcid.org/0000-0002-3369-4438

Michele Muccini − *Consiglio Nazionale delle Ricerche, Istituto per lo Studio dei Materiali Nanostrutturati (CNR-ISMN), 40129 Bologna, Italy;* orcid.org/0000-0003-0489-8316

Massimiliano Cavallini − *Consiglio Nazionale delle Ricerche, Istituto per lo Studio dei Materiali Nanostrutturati (CNR-ISMN), 40129 Bologna, Italy*

Complete contact information is available at: https://pubs.acs.org/10.1021/acsaelm.3c01379

Notes

The authors declare no competing financial interest.

https://doi.org/10.1021/acsaelm.3c01379
ACS Appl. Electron. Mater. 2023, 5, 6996−7003

■ ACKNOWLEDGMENTS

D.G. acknowledges support from the CNR via Progetti di Ricerca@CNR (NOENDCAT). M.B. and M.M. acknowledge support from Italian PNRR MUR project ECS_00000033_E-COSISTER. The authors would like to acknowledge Federico Bona (CNR-ISMN) for valuable technical support.

■ REFERENCES

(1) Guo, X.; Facchetti, A. The journey of conducting polymers from discovery to application. *Nat. Mater.* **2020**, *19* (9), 922−928.
(2) Fratini, S.; Nikolka, M.; Salleo, A.; Schweicher, G.; Sirringhaus, H. Charge transport in high-mobility conjugated polymers and molecular semiconductors. *Nat. Mater.* **2020**, *19* (5), 491−502.
(3) Ostroverkhova, O. Organic Optoelectronic Materials: Mechanisms and Applications. *Chem. Rev.* **2016**, *116* (22), 13279−13412.
(4) Ostroverkhova, O. *Handbook of organic materials for electronic and photonic devices*; Woodhead Publishing: 2018.
(5) Muccini, M. A bright future for organic field-effect transistors. *Nat. Mater.* **2006**, *5* (8), 605−613.
(6) Bolognesi, M.; Prosa, M.; Toerker, M.; Sanchez, L. L.; Wieczorek, M.; Giacomelli, C.; Benvenuti, E.; Pellacani, P.; Elferink, A.; Morschhauser, A.; Sola, L.; Damin, F.; Chiari, M.; Whatton, M.; Haenni, E.; Kallweit, D.; Marabelli, F.; Peters, J.; Toffanin, S. A fully Integrated Miniaturized Optical Biosensor for Fast and Multiplexing Plasmonic Detection of high- and Low-molecular Weight Analytes. *Adv. Mater.* **2023**, *35* (26), No. 2208719.
(7) Prosa, M.; Benvenuti, E.; Kallweit, D.; Pellacani, P.; Toerker, M.; Bolognesi, M.; Lopez-Sanchez, L.; Ragona, V.; Marabelli, F.; Toffanin, S. Organic Light-Emitting Transistors in a Smart-Integrated System for Plasmonic-Based Sensing. *Adv. Funct. Mater.* **2021**, *31* (50), No. 2104927.
(8) Bronstein, H.; Nielsen, C. B.; Schroeder, B. C.; McCulloch, I. The role of chemical design in the performance of organic semiconductors. *Nat. Rev. Chem.* **2020**, *4* (2), 66−77.
(9) Melucci, M.; Durso, M.; Bettini, C.; Gazzano, M.; Maini, L.; Toffanin, S.; Cavallini, S.; Cavallini, M.; Gentili, D.; Biondo, V.; Generali, G.; Gallino, F.; Capelli, R.; Muccini, M. Structure-property relationships in multifunctional thieno(bis) imide-based semiconductors with different sized and shaped N-alkyl ends. *J. Mater. Chem. C* **2014**, *2* (17), 3448−3456.
(10) Gedefaw, D.; Prosa, M.; Bolognesi, M.; Seri, M.; Andersson, M. R. Recent Development of Quinoxaline Based Polymers/Small Molecules for Organic Photovoltaics. *Adv. Energy Mater.* **2017**, *7* (21), No. 1700575.
(11) Benvenuti, E.; Gentili, D.; Chiarella, F.; Portone, A.; Barra, M.; Cecchini, M.; Cappuccino, C.; Zambianchi, M.; Lopez, S. G.; Salzillo, T.; Venuti, E.; Cassinese, A.; Pisignano, D.; Persano, L.; Cavallini, M.; Maini, L.; Melucci, M.; Muccini, M.; Toffanin, S. Tuning polymorphism in 2,3-thienoimide capped oligothiophene based field-effect transistors by implementing vacuum and solution deposition methods. *J. Mater. Chem. C* **2018**, *6* (21), 5601−5608.
(12) Gentili, D.; Gazzano, M.; Melucci, M.; Jones, D.; Cavallini, M. Polymorphism as an additional functionality of materials for technological applications at surfaces and interfaces. *Chem. Soc. Rev.* **2019**, *48* (9), 2502−2517.
(13) Jacobs, I. E.; Moule, A. J. Controlling Molecular Doping in Organic Semiconductors. *Adv. Mater.* **2017**, *29* (42), No. 1703063.
(14) Scaccabarozzi, A. D.; Basu, A.; Anies, F.; Liu, J.; Zapata-Arteaga, O.; Warren, R.; Firdaus, Y.; Nugraha, M. I.; Lin, Y.; Campoy-Quiles, M.; Koch, N.; Muller, C.; Tsetseris, L.; Heeney, M.; Anthopoulos, T. D. Doping Approaches for Organic Semiconductors. *Chem. Rev.* **2022**, *122* (4), 4420−4492.
(15) Li, J.; Babuji, A.; Fijahi, L.; James, A. M.; Resel, R.; Salzillo, T.; Pfattner, R.; Ocal, C.; Barrena, E.; Mas-Torrent, M. Synergistic Effect of Solvent Vapor Annealing and Chemical Doping for Achieving High-Performance Organic Field-Effect Transistors with Ideal Electrical Characteristics. *ACS Appl. Mater. Interfaces* **2023**, *15* (4), 5521−5528.
(16) Ke, Z.; Ahmed, M. H.; Abtahi, A.; Hsu, S. H.; Wu, W.; Espenship, M. F.; Baustert, K. N.; Graham, K. R.; Laskin, J.; Pan, L.; Mei, J. Thermally Activated Aromatic Ionic Dopants (TA-AIDs) Enabling Stable Doping, Orthogonal Processing and Direct Patterning. *Adv. Funct. Mater.* **2022**, *33* (8), No. 2211522.
(17) Zhong, Y.; Untilova, V.; Muller, D.; Guchait, S.; Kiefer, C.; Herrmann, L.; Zimmermann, N.; Brosset, M.; Heiser, T.; Brinkmann, M. Preferential Location of Dopants in the Amorphous Phase of Oriented Regioregular Poly(3-hexylthiophene-2,5-diyl) Films Helps Reach Charge Conductivities of 3000 S cm−1. *Adv. Funct. Mater.* **2022**, *32* (30), No. 2202075.
(18) Tripathi, A.; Lee, Y.; Lee, S.; Woo, H. Y. Recent advances in n-type organic thermoelectric materials, dopants, and doping strategies. *J. Mater. Chem. C* **2022**, *10* (16), 6114−6140.
(19) Xu, Y.; Sun, H.; Liu, A.; Zhu, H.-H.; Li, W.; Lin, Y.-F.; Noh, Y.-Y. Doping: A Key Enabler for Organic Transistors. *Adv. Mater.* **2018**, *30* (46), No. 1801830.
(20) Lussem, B.; Keum, C. M.; Kasemann, D.; Naab, B.; Bao, Z.; Leo, K. Doped Organic Transistors. *Chem. Rev.* **2016**, *116* (22), 13714−13751.
(21) Pschenitzka, F.; Sturm, J. C. Solvent-enhanced dye diffusion in polymer thin films for color tuning of organic light-emitting diodes. *Appl. Phys. Lett.* **2001**, *78* (17), 2584−2586.
(22) Graves-Abe, T.; Pschenitzka, F.; Jin, H. Z.; Bollman, B.; Sturm, J. C.; Register, R. A. Solvent-enhanced dye diffusion in polymer thin films for polymer light-emitting diode application. *J. Appl. Phys.* **2004**, *96* (12), 7154−7163.
(23) Wu, C.-C.; Lin, S.-W.; Chen, C.-W.; Hsu, J.-H. Solvent-assisted dye-diffusion thermal transfer for electronic imaging applications. *Appl. Phys. Lett.* **2002**, *80* (7), 1117−1119.
(24) Lee, B. H.; Bazan, G. C.; Heeger, A. J. Doping-Induced Carrier Density Modulation in Polymer Field-Effect Transistors. *Adv. Mater.* **2016**, *28* (1), 57−62.
(25) Sakai, N.; Warren, R.; Zhang, F.; Nayak, S.; Liu, J.; Kesava, S. V.; Lin, Y. H.; Biswal, H. S.; Lin, X.; Grovenor, C.; Malinauskas, T.; Basu, A.; Anthopoulos, T. D.; Getautis, V.; Kahn, A.; Riede, M.; Nayak, P. K.; Snaith, H. J. Adduct-based p-doping of organic semiconductors. *Nat. Mater.* **2021**, *20* (9), 1248−1254.
(26) He, T.; Stolte, M.; Wang, Y.; Renner, R.; Ruden, P. P.; Wurthner, F.; Frisbie, C. D. Site-specific chemical doping reveals electron atmospheres at the surfaces of organic semiconductor crystals. *Nat. Mater.* **2021**, *20* (11), 1532−1538.
(27) Kolesov, V. A.; Fuentes-Hernandez, C.; Chou, W. F.; Aizawa, N.; Larrain, F. A.; Wang, M.; Perrotta, A.; Choi, S.; Graham, S.; Bazan, G. C.; Nguyen, T. Q.; Marder, S. R.; Kippelen, B. Solution-based electrical doping of semiconducting polymer films over a limited depth. *Nat. Mater.* **2017**, *16* (4), 474−480.
(28) Pingel, P.; Arvind, M.; Kölln, L.; Steyrleuthner, R.; Kraffert, F.; Behrends, J.; Janietz, S.; Neher, D. p-Type Doping of Poly(3-hexylthiophene) with the Strong Lewis Acid Tris(pentafluorophenyl)-borane. *Adv. Electron. Mater.* **2016**, *2* (10), No. 1600204.
(29) Panidi, J.; Paterson, A. F.; Khim, D.; Fei, Z.; Han, Y.; Tsetseris, L.; Vourlias, G.; Patsalas, P. A.; Heeney, M.; Anthopoulos, T. D. Remarkable Enhancement of the Hole Mobility in Several Organic Small-Molecules, Polymers, and Small-Molecule:Polymer Blend Transistors by Simple Admixing of the Lewis Acid p-Dopant B(C6F5)3. *Adv. Sci.* **2018**, *5* (1), No. 1700290.
(30) Yurash, B.; Cao, D. X.; Brus, V. V.; Leifert, D.; Wang, M.; Dixon, A.; Seifrid, M.; Mansour, A. E.; Lungwitz, D.; Liu, T.; Santiago, P. J.; Graham, K. R.; Koch, N.; Bazan, G. C.; Nguyen, T. Q. Towards understanding the doping mechanism of organic semiconductors by Lewis acids. *Nat. Mater.* **2019**, *18* (12), 1327−1334.
(31) Gentili, D.; Di Maria, F.; Liscio, F.; Ferlauto, L.; Leonardi, F.; Maini, L.; Gazzano, M.; Milita, S.; Barbarella, G.; Cavallini, M. Targeting ordered oligothiophene fibers with enhanced functional properties by interplay of self-assembly and wet lithography. *J. Mater. Chem.* **2012**, *22* (39), 20852−20856.
(32) Gentili, D.; Givaja, G.; Mas-Balleste, R.; Azani, M.-R.; Shehu, A.; Leonardi, F.; Mateo-Marti, E.; Greco, P.; Zamora, F.; Cavallini, M.

https://doi.org/10.1021/acsaelm.3c01379
ACS Appl. Electron. Mater. 2023, 5, 6996−7003

Patterned conductive nanostructures from reversible self-assembly of 1D coordination polymer. *Chem. Sci.* **2012**, *3* (6), 2047−2051.
(33) Pschenitzka, F.; Sturm, J. C. Three-color organic light-emitting diodes patterned by masked dye diffusion. *Appl. Phys. Lett.* **1999**, *74* (13), 1913−1915.
(34) Kazuya Tada, K. T.; Mitsuyoshi Onoda, M. O. Three-Color Polymer Light-Emitting Devices Patterned by Maskless Dye Diffusion onto Prepatterned Electrode. *Jpn. J. Appl. Phys.* **1999**, *38* (10A), L1143.
(35) Nakamura, A.; Tada, T.; Mizukami, M.; Hirose, S.; Yagyu, S. Three-color polymer light-emitting diodes by stamped dye diffusion. *Appl. Phys. Lett.* **2002**, *80* (12), 2189−2191.
(36) Khim, D.; Baeg, K.-J.; Caironi, M.; Liu, C.; Xu, Y.; Kim, D.-Y.; Noh, Y.-Y. Control of Ambipolar and Unipolar Transport in Organic Transistors by Selective Inkjet-Printed Chemical Doping for High Performance Complementary Circuits. *Adv. Funct. Mater.* **2014**, *24* (40), 6252−6261.
(37) Perevedentsev, A.; Campoy-Quiles, M. Rapid and high-resolution patterning of microstructure and composition in organic semiconductors using 'molecular gates'. *Nat. Commun.* **2020**, *11* (1), 3610.
(38) Tada, K.; Onoda, M. Green- and White-Light-Emitting Devices Made from Poly(9,9-dioctylfluorene) by Maskless Dye Diffusion Technique. *Jpn. J. Appl. Phys.* **2005**, *44* (6R), 4167−4170.
(39) Tada, K.; Onoda, M. Red emission from poly(9,9-dioctylfluorene) doped with phosphorescent dye through maskless dye-diffusion technique. *Appl. Phys. Lett.* **2006**, *89* (4), No. 043508.
(40) Long, K.; Pschenitzka, F.; Sturm, J. C. Three-Color Passive-Matrix Pixels Using Dye-Diffusion-Patterned Tri-Layer Polymer-Based LED. *MRS Online Proc. Library (OPL)* **2001**, *708*, BB6.8.
(41) Jacobs, I. E.; Aasen, E. W.; Nowak, D.; Li, J.; Morrison, W.; Roehling, J. D.; Augustine, M. P.; Moule, A. J. Direct-Write Optical Patterning of P3HT Films Beyond the Diffraction Limit. *Adv. Mater.* **2017**, *29* (2), No. 1603221.
(42) Qin, D.; Xia, Y.; Whitesides, G. M. Soft lithography for micro- and nanoscale patterning. *Nat. Protoc.* **2010**, *5* (3), 491−502.
(43) Nečas, D.; Klapetek, P. Gwyddion: an open-source software for SPM data analysis. *Cent. Eur. J. Phys.* **2012**, *10* (1), 181−188.
(44) Liu, Y.; Zhang, L.; Mo, C.; Cao, Y.; Wu, W.; Wang, W. Caulking polydimethylsiloxane molecular networks by thermal chemical vapor deposition of Parylene-C. *Lab Chip* **2016**, *16* (21), 4220−4229.
(45) Shirure, V. S.; George, S. C. Design considerations to minimize the impact of drug absorption in polymer-based organ-on-a-chip platforms. *Lab Chip* **2017**, *17* (4), 681−690.
(46) Xia, Y. N.; Whitesides, G. M. Soft lithography. *Angew. Chem., Int. Ed.* **1998**, *37* (5), 551−575.
(47) Jacobs, I. E.; Aasen, E. W.; Oliveira, J. L.; Fonseca, T. N.; Roehling, J. D.; Li, J.; Zhang, G.; Augustine, M. P.; Mascal, M.; Moulé, A. J. Comparison of solution-mixed and sequentially processed P3HT:F4TCNQ films: effect of doping-induced aggregation on film morphology. *J. Mater. Chem. C* **2016**, *4* (16), 3454−3466.
(48) Mun, J.; Kang, J.; Zheng, Y.; Luo, S.; Wu, Y.; Gong, H.; Lai, J. C.; Wu, H. C.; Xue, G.; Tok, J. B. H.; Bao, Z. F4-TCNQ as an Additive to Impart Stretchable Semiconductors with High Mobility and Stability. *Adv. Electron. Mater.* **2020**, *6* (6), No. 2000251.
(49) Wang, Z.; Zou, Y.; Chen, W.; Huang, Y.; Yao, C.; Zhang, Q. The Role of Weak Molecular Dopants in Enhancing the Performance of Solution-Processed Organic Field-Effect Transistors. *Adv. Electron. Mater.* **2018**, *5* (2), No. 1800547.
(50) Yee, P. Y.; Scholes, D. T.; Schwartz, B. J.; Tolbert, S. H. Dopant-Induced Ordering of Amorphous Regions in Regiorandom P3HT. *J. Phys. Chem. Lett.* **2019**, *10* (17), 4929−4934.
(51) Lim, E.; Glaudell, A. M.; Miller, R.; Chabinyc, M. L. The Role of Ordering on the Thermoelectric Properties of Blends of Regioregular and Regiorandom Poly(3-hexylthiophene). *Adv. Electron. Mater.* **2019**, *5* (11), No. 1800915.
(52) Bourson, J.; Valeur, B. Ion-responsive fluorescent compounds. 2. Cation-steered intramolecular charge transfer in a crowned merocyanine. *J. Phys. Chem.* **1989**, *93* (9), 3871−3876.
(53) Tang, C. W.; VanSlyke, S. A.; Chen, C. H. Electroluminescence of doped organic thin films. *J. Appl. Phys.* **1989**, *65* (9), 3610−3616.
(54) Manna, B. Temperature dependence of resonance energy transfer in DCM doped anthracene nanoaggregates. *J. Lumin.* **2019**, *209*, 379−386.

https://doi.org/10.1021/acsaelm.3c01379
ACS Appl. Electron. Mater. 2023, 5, 6996−7003